Multiscale Analysis of Complex Time Series: Integration of Chaos and Random Fractal Theory, and Beyond
by Jianbo Gao, Yinhe Cao, Wen-wen Tung and Jing Hu

CHAPTER 14

POWER-LAW SENSITIVITY TO INITIAL CONDITIONS (PSIC) — AN INTERESTING CONNECTION BETWEEN CHAOS THEORY AND RANDOM FRACTAL THEORY

Chaos theory shows that apparently irregular behaviors in a complex system may be generated by nonlinear deterministic interactions of only a few numbers of degrees of freedom. Noise or intrinsic randomness does not play any role. Random fractal theory, on the other hand, assumes that the dynamics of the system are inherently random. Since the foundations of chaos theory and random fractal theory are entirely different, different conclusions may be drawn, depending upon which theory is used to analyze the data. In fact, as we explained in Chapter 13, much of the research in the past was devoted to determining whether a complex time series is generated by a chaotic or a random system. Such a categorical study, however, may discourage cross-talks between researchers specializing in chaos theory and random fractal theory, hindering the development of new methods for the multiscale analysis of complex data. Therefore, it would be very desirable to develop a more general framework to encompass chaos theory and random fractal theory as special cases. In this chapter, we show that power-law sensitivity to initial conditions (PSIC) provides such a framework.

14.1 EXTENDING EXPONENTIAL SENSITIVITY TO INITIAL CONDITIONS TO PSIC

As we have shown in Chapter 13, deterministic chaos is defined by exponential sensitivity to initial conditions (ESIC). In order to characterize a type of motion whose complexity is neither regular nor fully chaotic/random, recently the concept of ESIC has been generalized to PSIC by Tsallis and co-workers [450]. Mathematically, the formulation of PSIC closely parallels that of nonextensive entropy formalism, as briefly described in Sec. 11.1.4. In particular, there is also a parameter, the entropic index q, in PSIC. However, as will be explained momentarily, q in PSIC and q in Tsallis entropy are not the same.

To understand the essence of PSIC, let us focus on the one-dimensional case and consider

$$\xi(t) = \lim_{\Delta x(0)\to 0} \frac{\Delta x(t)}{\Delta x(0)},$$

where $\Delta x(0)$ is the infinitesimal discrepancy in the initial condition and $\Delta x(t)$ is the discrepancy at time $t > 0$. When the motion is chaotic, then

$$\xi(t) = e^{\lambda_1 t}.$$

$\xi(t)$ satisfies

$$\frac{d\xi(t)}{dt} = \lambda_1 \xi(t). \tag{14.1}$$

Tsallis and co-workers have generalized Eq. (14.1) to

$$\frac{d\xi(t)}{dt} = \lambda_q \xi(t)^q, \tag{14.2}$$

where q is called the entropic index, and λ_q is interpreted to be equal to K_q, the generalization of the KS entropy. Equation (14.2) defines the PSIC in the one-dimensional case. Obviously, PSIC reduces to ESIC when $q \to 1$. The solution to Eq. (14.2) is

$$\xi(t) = [1 + (1-q)\lambda_q t]^{1/(1-q)}. \tag{14.3}$$

Notice the striking similarity between Eq. (14.3) and Eqs. (11.21) and (11.23), which give Tsallis and generalized Tsallis distributions. When t is large and $q \neq 1$, $\xi(t)$ increases with t as a power law,

$$\xi(t) \sim C t^{1/(1-q)}, \tag{14.4}$$

where $C = [(1-q)\lambda_q]^{1/(1-q)}$. For Eq. (14.4) to define an unstable motion with $\lambda_q > 0$, we must have $q \leq 1$. In contrast, in Tsallis entropy, $-\infty < q < \infty$. Therefore, q in PSIC and q in Tsallis entropy are different. Below we shall map different types of motions to different ranges of q.

To apply PSIC to the analysis of time series data, one can first construct a phase space by constructing embedding vectors, $V_i = [x(i), x(i+L), \cdots, x(i+(m-$

$1)L)]$, where $x(i), i = 1, 2, \cdots$ is the given scalar time series. Equation (14.3) can then be generalized to the high-dimensional case,

$$\xi(t) = \lim_{||\Delta V(0)|| \to 0} \frac{||\Delta V(t)||}{||\Delta V(0)||} = \left[1 + (1-q)\lambda_q^{(1)} t\right]^{1/(1-q)}, \tag{14.5}$$

where $||\Delta V(0)||$ is the infinitesimal discrepancy between two orbits at time 0, $||\Delta V(t)||$ is the distance between the two orbits at time $t > 0$, q is the entropic index, and $\lambda_q^{(1)}$ is the first q-Lyapunov exponent, corresponding to the power-law increase of the first principal axis of an infinitesimal ball in the phase space. $\lambda_q^{(1)}$ may not be equal to K_q. This is understood by recalling that for chaotic systems, the KS entropy is the sum of all the positive Lyapunov exponents. We believe that a similar relation may hold between the q-Lyapunov exponents and K_q. When there are multiple unstable directions, then in general $\lambda_q^{(1)}$ may not be equal to K_q. When t is large and $q \neq 1$, Eq. (14.5) again gives a power-law increase of $\xi(t)$ with t.

We now consider the general computational framework for PSIC. Given a finite time series, the condition of $||\Delta V(0)|| \to 0$ cannot be satisfied. In order to find the law governing the divergence of nearby orbits, one has to examine how the neighboring points, (V_i, V_j), in the phase space evolve with time by forming suitable ensemble averages. Notice that if (V_{i1}, V_{j1}) and (V_{i2}, V_{j2}) are two pairs of nearby points, when $||V_{i1} - V_{j1}|| \ll ||V_{i2} - V_{j2}|| \ll 1$, the separations such as $||V_{i1+t} - V_{j1+t}||$ and $||V_{i2+t} - V_{j2+t}||$ cannot be simply averaged to provide estimates for q and $\lambda_q^{(1)}$. In fact, it would be most convenient to consider ensemble averages of pairs of points (V_i, V_j) that all fall within a very thin shell, $r_1 \leq ||V_i - V_j|| \leq r_2$, where r_1 and r_2 are close. These arguments suggest that the time-dependent exponent curves defined by Eq. (13.5) provide a natural framework to assess PSIC from a time series. This is indeed so. In fact, we have

$$\ln \xi(t) \approx \Lambda(t) = \left\langle \ln \left(\frac{||X_{i+t} - X_{j+t}||}{||X_i - X_j||} \right) \right\rangle . \tag{14.6}$$

Now, by the discussions in Chapter 13, it is clear that PSIC is a generalization of ESIC: As long as the $\Lambda(t)$ curves from different shells form a linear envelope, $q = 1$ and the motion is chaotic. The next question is: Does PSIC also include random fractals as special cases? The answer is yes. This will be shown in the next section. There we will also gain a better understanding of the meaning of $\lambda_q^{(1)}$.

14.2 CHARACTERIZING RANDOM FRACTALS BY PSIC

As we have discussed in Chapters 7 and 8, Levy processes and $1/f^{\beta}$ processes with long-range correlations constitute two major types of random fractals. Below we show, both analytically and through numerical simulations, that both types of processes can be readily characterized by PSIC.

14.2.1 Characterizing $1/f^{\beta}$ processes by PSIC

In Chapters 6 and 8, we demonstrated the ubiquity of $1/f^{\beta}$ processes in science and engineering. Two important prototypical models for such processes are the fractional Brownian motion (fBm) processes and ON/OFF intermittency with power-law distributed ON and OFF periods, discussed in Chapters 6 and 8, respectively. To put $1/f^{\beta}$ processes in the framework of PSIC, as before, we introduce a parameter H through the equation

$$\beta = 2H + 1, \quad 0 < H < 1.$$

The defining property for a $1/f^{\beta}$ process is that its variance increases with t as t^{2H}. Irrespective of which embedding dimension is chosen, this property can be translated into

$$\xi(t) = t^{H} . \tag{14.7}$$

Therefore,

$$\frac{d\xi(t)}{dt} = Ht^{H-1} . \tag{14.8}$$

Expressing t in terms of ξ, we have

$$\frac{d\xi(t)}{dt} = H\xi^{1-\frac{1}{H}} . \tag{14.9}$$

Comparing with the defining Eq. (14.2) of PSIC, we find that

$$q = 1 - \frac{1}{H} = 1 - \frac{2}{\beta - 1}, \tag{14.10}$$

$$\lambda_q^{(1)} = H = \frac{\beta - 1}{2} . \tag{14.11}$$

Noting that $0 < H < 1$, from Eq. (14.10) we have $-\infty < q < 0$.

Computationally, the key is to demonstrate the behaviors described by Eq. (14.7). This can be readily done by calculating the time-dependent exponent curves defined by Eq. (14.6) (see also Eq. (13.5)). Let us first examine the fBm processes. Figure 14.1 shows three examples for the fBm processes with $H = 0.25, 0.5$, and 0.75. Clearly, the slopes of the straight lines correctly estimate the H parameter used in the simulations.

Next, we examine ON/OFF processes with Pareto-distributed ON and OFF periods as that described by Eq. (3.24). Figure 14.2 shows three examples for $\mu = 1.2, 1.6$, and 2.0. Noting that $H = (3 - \mu)/2$, we see that the slopes of the straight lines again correctly estimate the H parameter. Also note that when $0 < \mu < 1, 1 < H < 1.5$. Therefore, Eqs. (14.7) and (14.10) are still correct when $1 < H < 1.5$. The entire range of $H = (3 - \mu)/2$, with $0 < \mu \leq 2$, determines that $-1 \leq q < 1/3$ for Pareto-distributed ON/OFF processes.

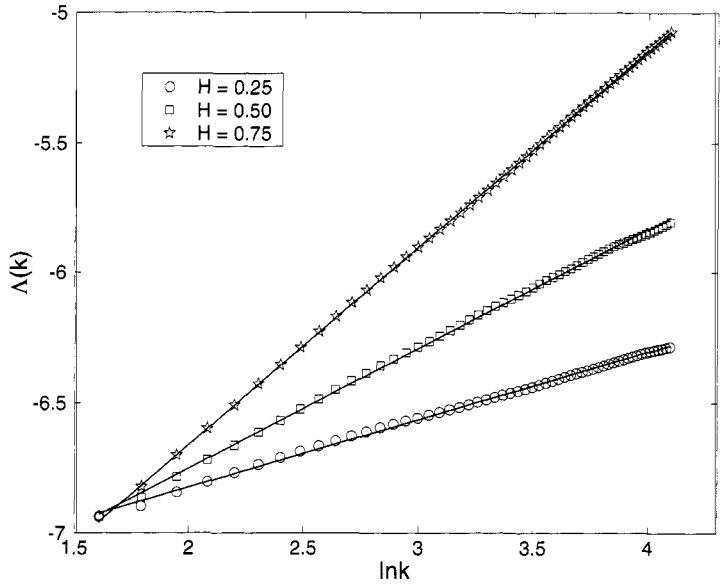

Figure 14.1. $\Lambda(k)$ vs. $\ln k$ curves for fBm.

14.2.2 Characterizing Levy processes by PSIC

In Chapter 7, we discussed α-stable distributions and Levy processes. To clarify the following discussions, we briefly review the major elements in Chapter 7.

A (standard) symmetric α-stable Levy process $\{L_\alpha(t), t \geq 0\}$ is a stochastic process that is almost surely zero at $t = 0$, has independent increments, and $L_\alpha(t) - L_\alpha(s)$ follows an α-stable distribution with characteristic function $e^{-(t-s)|u|^\alpha}$, where $0 \leq s < t < \infty$. Equation (7.7) shows that a random variable Y is called (strictly) stable if the distribution for $\sum_{i=1}^n Y_i$ is the same as that for $n^{1/\alpha}Y$,

$$\sum_{i=1}^{n} Y_i \stackrel{d}{=} n^{1/\alpha} Y,$$

where $Y_1, Y_2, \cdots$ are independent random variables, each having the same distribution as Y. This means that $n\text{Var}Y = n^{2/\alpha}\text{Var}Y$. For the distribution to be valid, $0 < \alpha \leq 2$. When $\alpha = 2$, the distribution is Gaussian, and hence, the corresponding Levy process is just the standard Brownian motion (Bm). When $0 < \alpha < 2$, the distribution is heavy-tailed, $P[X \geq x] \sim x^{-\alpha}$, $x \to \infty$, and has infinite variance. Furthermore, when $0 < \alpha \leq 1$, the mean is also infinite.

The symmetric α-stable Levy motion is $1/\alpha$ self-similar. That is, for $c > 0$, the processes $\{L_\alpha(ct), t \geq 0\}$ and $\{c^{1/\alpha}L_\alpha(t), t \geq 0\}$ have the same finite-dimensional distributions. By this argument as well as Eq. (7.7), it is clear that the length of the motion in a time span of Δt, $\Delta L(\Delta t)$ is given by the following scaling:

$$\Delta L(\Delta t) \propto \Delta t^{1/\alpha}. \tag{14.12}$$

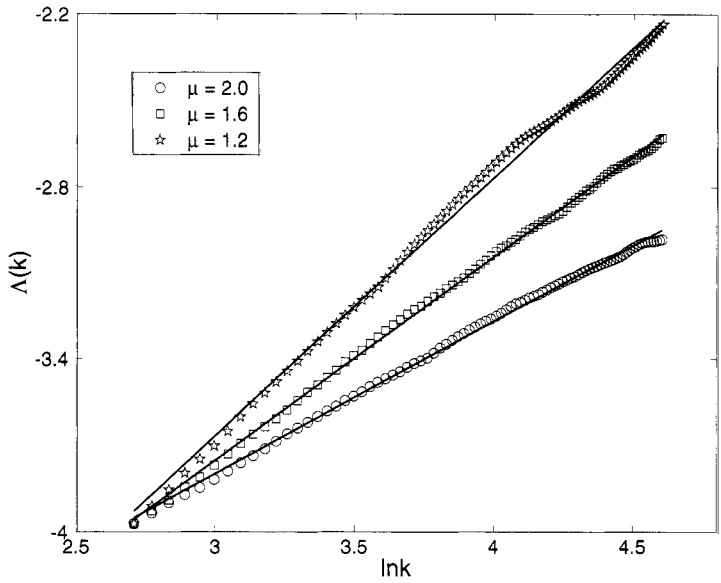

Figure 14.2. $\Lambda(k)$ vs. $\ln k$ curves for ON/OFF model.

Comparing to $1/f^{2H+1}$ processes, we identify that $1/\alpha$ plays the role of H. Therefore,

$$q = 1 - \alpha, \tag{14.13}$$

$$\lambda_q^{(1)} = 1/\alpha. \tag{14.14}$$

Noting that $0 < \alpha \leq 2$, from Eq. (14.13) we have $-1 \leq q < 1$.

We have simulated a number of Levy processes with different α. Examples for $\alpha = 1$ and 1.5 are shown in Fig. 14.3. The slopes of the straight lines correctly estimate the values of α used in the simulations.

14.3 CHARACTERIZING THE EDGE OF CHAOS BY PSIC

In nature and in engineering, many types of motion are neither regular nor fully chaotic/random. An example is motions around the edge of chaos. The ubiquity of such motions is perhaps the reason that truly chaotic dynamics have rarely been observed in time series data. To qualify as a unified theory, PSIC must be able to characterize such types of motion. Pleasingly, this can be done, as illustrated by the following discussions on the deterministic and noisy logistic map:

$$x_{n+1} = ax_n(1 - x_n) + \sigma\eta_n, \tag{14.15}$$

where a is the bifurcation parameter and η_n is a white Gaussian noise with mean 0 and variance 1. The parameter σ characterizes the strength of noise. For the

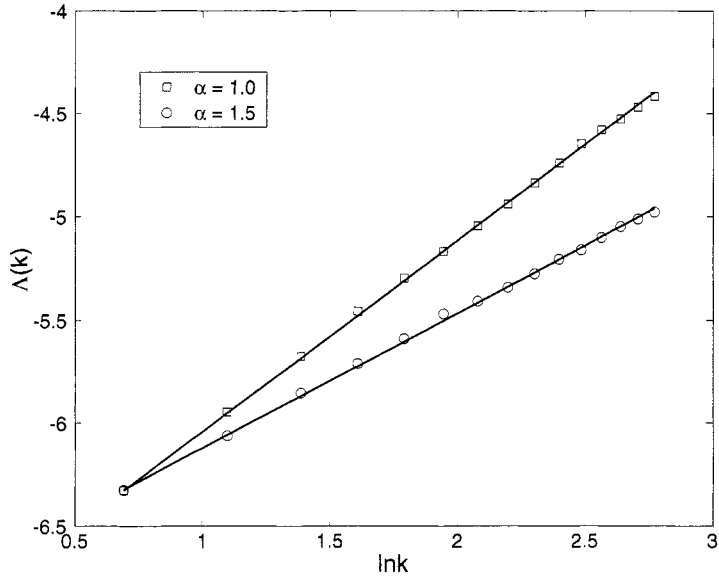

Figure 14.3. $\Lambda(k)$ vs. $\ln k$ curves for Levy flights.

clean system ($\sigma = 0$), the edge of chaos occurs at the accumulation point, $a_\infty = 3.569945672\cdots$. We shall study three parameter values: $a_1 = a_\infty - 0.001$, a_∞, and $a_2 = a_\infty + 0.001$. When noise is absent, a_1 corresponds to a periodic motion with period 2^5, while a_2 corresponds to a truly chaotic motion. We shall only study transient-free time series. In Figs. 14.4(a–c), we have plotted the $\Lambda(t)$ vs. t curves for parameter values a_1, a_∞, and a_2, respectively. We observe in Fig. 14.4(a) that the variation of $\Lambda(t)$ with t is periodic (with period 16, which is half of the period of the motion) when the motion is periodic. This is a generic feature of the $\Lambda(t)$ curves for discrete periodic attractors when the radius of the shell is larger than the smallest distance between two points on the attractor (when a periodic attractor is continuous, $\Lambda(t)$ can be arbitrarily close to zero).

Tsallis and co-workers found that at the edge of chaos for the logistic map, $\xi(t)$ is given by Eq. (14.3) with $q \approx 0.2445$. Surprisingly, we do not observe such a divergence in Fig. 14.4(b). In fact, if one plots $\Lambda(t)$ vs. $\ln t$, one only observes a curve that increases very slowly. The more interesting pattern is the one shown in Fig. 14.4(c), where we observe a linearly increasingly $\Lambda(t)$ vs. t curve. In fact, Fig. 14.4(c) shows two such curves corresponding to two different shells. Interestingly, the two curves collapse to form a common envelope in the linearly increasing part of the curve. The slope of the envelope gives a good estimate of the largest positive Lyapunov exponent. This is a generic feature of chaos, as explained in Chapter 13. Since the chaos studied here is close to the edge of chaos, the curves shown in Fig. 14.4(c) are less smooth than those discussed earlier.

Why can the theoretical prediction of PSIC at the edge of chaos for the logistic map not be observed from a clean time series? It turns out that the existence of dynamic noise is the key to observe PSIC in time series data. This is illustrated in Figs. 14.4(d–f), where we have shown the $\Lambda(t)$ vs. $\ln t$ curves for the three parameters considered, with noise strength $\sigma_1 = 0.001$. In fact, each figure shows two curves corresponding to two different shells. The curves parallel each other. The slopes of those curves are about 1.20, close to the theoretical value of $1/(1 - 0.2445) \approx 1.32$. While it is very satisfactory to observe PSIC at the edge of chaos, it is more thrilling to observe the collapse of regular as well as chaotic motions onto the PSIC attractor around the edge of chaos. This signifies the stability of PSIC when there is dynamic noise. It is important to emphasize that the results shown in Figs. 14.4(d–f) are largely independent of noise strength, so long as the noise is neither too weak nor too strong. For example, very similar results have been observed with $\sigma_2 = \sigma_1/10 = 0.0001$.

We note that similar results can be readily obtained in higher-dimensional systems, such as the two-dimensional Henon map. While these studies demonstrate the ubiquity of PSIC, they also highlight the importance of dynamic noise. The existence of the latter is perhaps the very reason that truly chaotic time series can seldom be observed.

In closing this section, we note that the edge of chaos is characterized by $q \approx 0.2445$, which is larger than 0 but smaller than 1.

14.4 BIBLIOGRAPHIC NOTES

Most of the materials discussed here have not appeared elsewhere. They have been developed based on [176, 289, 450]. See also [56, 85, 276, 436–441] on applications of PSIC in model dynamical systems. Note that the formalism of PSIC closely parallels that of nonextensive statistical mechanics (NESM) of Tsallis [448], which has found numerous applications to the study of systems with long-range interactions [12, 277, 278, 349], multifractal behavior [13, 289], and fully developed turbulence [13, 37, 38], among many others.

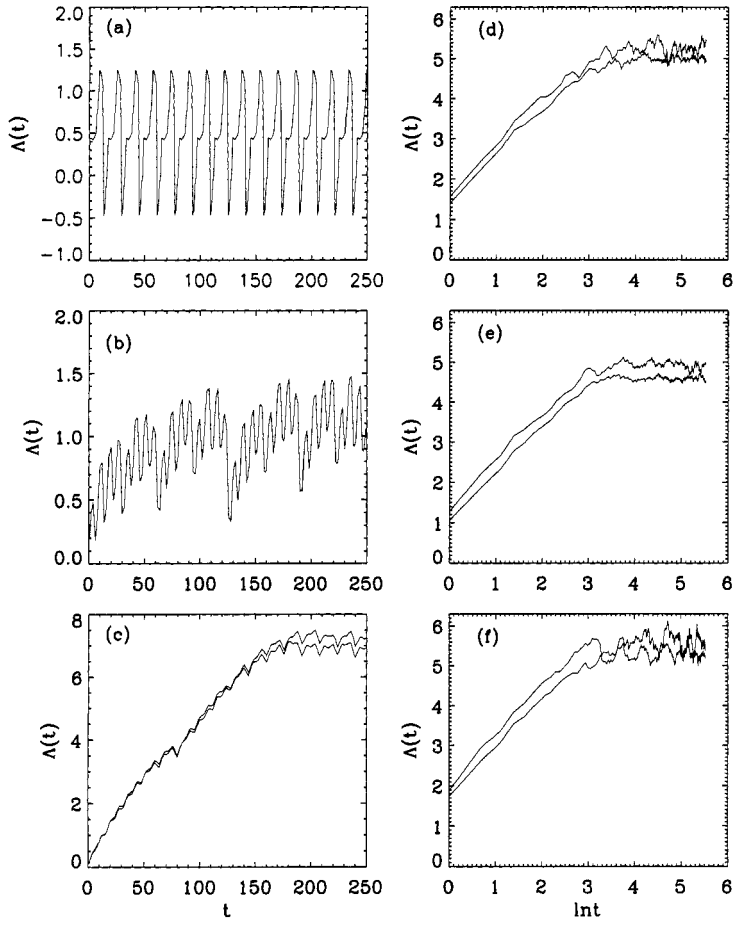

Figure 14.4. $\Lambda(t)$ vs. t curves for time series generated from the noise-free logistic map with (a) $a_1 = a_\infty - 0.001$, where the motion is periodic with period 2^5, (b) $a_\infty = 3.569945672\cdots$, and (c) $a_2 = a_\infty + 0.001$, where the motion is chaotic. Plotted in (d–f) are $\Lambda(t)$ vs. $\ln t$ curves for the noisy logistic map with $\sigma = 0.001$. Very similar results were obtained when $\sigma = 0.0001$. Shown in (c–f) are two curves corresponding to two different shells. A total of 10^4 points were used in the computation, with embedding parameters $m = 4$, $L = 1$. However, so long as $m > 1$, the results are largely independent of embedding. When $m = 1$, the $\Lambda(t)$ curves are not smooth, and the estimated $1/(1-q)$ is much smaller than the theoretical value.